Development of a Six-Axis Force/Moment Sensor with Rectangular Taper Beams for an Intelligent Robot

Gab-Soon Kim

Abstract: This paper describes the development of a six-axis force/moment sensor with rectangular taper beams for an intelligent robot's wrist and ankle. In order to accurately push and pull an object with an intelligent robot's hand, and in order to safely walk with an intelligent robot's foot, the robot's wrist and ankle should measure three forces Fx, Fy, and Fz, and three moments Mx, My, and Mz simultaneously from the mounted six-axis force/moment sensor to the intelligent robot's wrist and ankle. Unfortunately, the developed six-axis force/moment sensor utilized in other industrial fields is not proper for an intelligent robot's wrist and ankle in the size and the rated output of the six-axis force/moment sensor. In this paper, the structure of a six-axis force/moment sensor with rectangular taper beams was newly modeled for an intelligent robot's wrist and ankle, and the sensing elements were designed by using the derived equations, following which the six-axis force/moment sensor was fabricated by attaching strain-gages on the sensing elements. Moreover, the characteristic test of the developed sensor was carried out by using the six-component force/moment sensor testing machine. The rated outputs from the derived equations agree well with those from the experiments. The interference error of the sensor is less than 2.87%.

Keywords: Humanoid robot, intelligent robot, intelligent robot's foot, intelligent robot's ankle, interference error, rated output, six-axis force/moment sensor.

1. INTRODUCTION

Scientists have been researching the development of an intelligent robot because it is desired to obtain a mechanism that can work for a human being. An intelligent robot's hand (wrist) [1-4] should measure three forces Fx, Fy, and Fz and three moments Mx, My, and Mz simultaneously from the attached six-axis force/moment sensor to between its hand and arm for pushing and pulling an object. Also, an intelligent robot's foot (ankle) [5-8] should measure three forces Fx, Fy, and Fz and three moments Mx, My, and Mz simultaneously from the attached six-axis force/moment sensor to between its foot and leg for walking on uneven terrains. Unfortunately, the developed six-axis force/moment sensor utilized for other industrial fields is not proper for an intelligent robot's wrist and ankle primarily due to the size and the rated output of the sensor.

Kim [9-11] developed some kind of a six-axis force/moment sensor with interference error of less than 3%, but it cannot be mounted to an intelligent robot because of its inappropriate size. The sensing elements of the developed sensors have the disadvantage that it is difficult to design the sensor with various rated outputs and loads. The United States and Japan [12] have already developed and handled many kinds of six-axis force/torque sensors, but they are expensive and are not suitable to be mounted to a special intelligent robot's wrist and ankle. Therefore, it is necessary to develop the six-axis force/moment sensor with new structure for an intelligent robot's wrist and ankle.

The six-axis force/moment sensor that is composed of Fx sensor, Fy sensor, Fz sensor, Mx sensor, My sensor and Mz sensor should be designed and fabricated in a body to reduce interference error. And, it should have the proper rated load and size, as well as an interference error of below 3% for better accuracy of the intelligent robot. The accuracy of the six-axis force/moment sensor signifies the interference error, because the interference error is much higher than the nonlinearity error, repeatability error, and hysteresis error [9-11].

A six-axis force/moment sensor with complex structure and many design variables is generally

Manuscript received June 12, 2006; revised January 15, 2007; accepted May 2, 2007. Recommended by Editorial Board member Sangdeok Park under the direction of Editor Jae-Bok Song. This work was supported by the Korea Science and Engineering Foundation (KOSEF) grant funded by the Korean government (MOST) (No. R01-2006-000-10468-0).

Gab-Soon Kim is with ERI, Department of Control and Instrumentation Engineering, Gyeongsang National University, 900 Gazwa-Dong, Jinju, Kyungnam 660-701, Korea (e-mail: gskim@gsnu.ac.kr).

designed by processing. First, the strain equations are derived. Second, the analysis program is made using the derived equations. Finally, the program is used to design a six-axis force/moment sensor [9-11].

In this paper, first, the structure of a six-axis force/moment sensor with rectangular taper beams was newly modeled for an intelligent robot's wrist and ankle. Second, the equations to predict the strains on the sensing elements were derived and the analysis program was made using the derived equations. Third, the size of the sensing elements was designed by using the equations. Forth, the six-axis force/moment sensor was fabricated by attaching strain-gages on the sensing elements, and finally, the characteristic test of the developed sensor was carried out by using the six-axis force/moment sensor calibration machine.

2. DESIGN OF A SIX-AXIS ANKLE FORCE/MOMENT SENSOR

2.1. Structure of sensing elements

Fig. 1 shows the structure of sensing elements of the six-axis force/moment sensor for the wrist and the ankle of an intelligent robot. The sensor is composed of a fixture ring, a force/moment transmitting block, fixture blocks FB1~4, moving blocks MB1~4, parallel-plate beams (PPBs) PPB1~8, and rectangular taper beams 1~4. The sizes of the rectangular taper beams with width b_1 and b_1', thickness t_1 and t_1', and length l_1, and the sizes of the parallel-plate

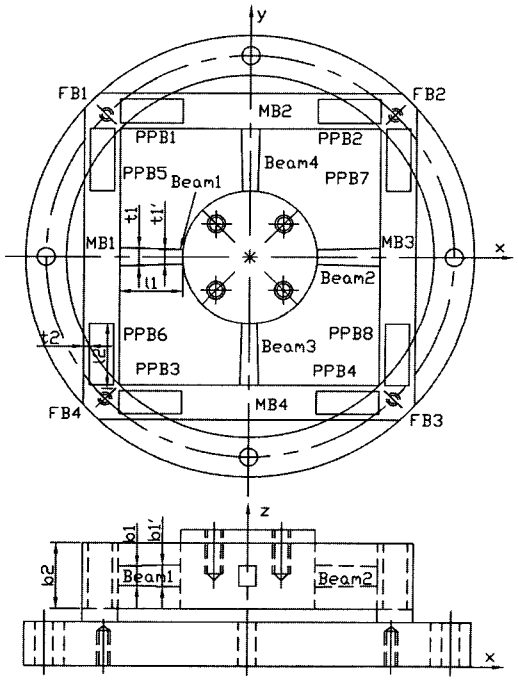

Fig. 1. Structure of sensing element for six-axis ankle force/moment sensor with rectangular taper beams.

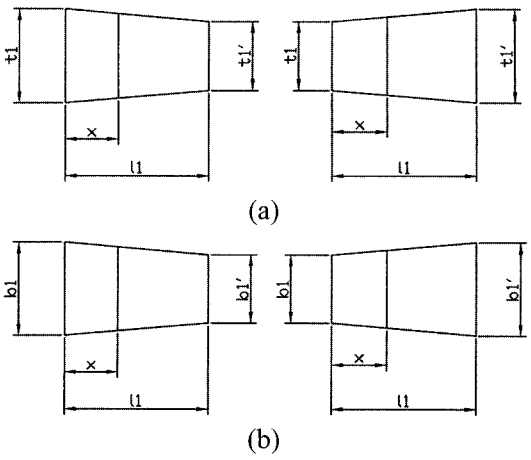

Fig. 2. Schematic diagram of sensing element (rectangular taper beam).

beams with width b_2, thickness t_2 and length l_2 are used as design variables for designing the sensor. In this paper, the rectangular taper beams 1~4 are used because of more advantage in the design of the sensor than the rectangular beam.

In order to determine the sizes of the rectangular taper beams and the parallel-plate beams, that is, to design the sensor, it is necessary for the beams to be analyzed by strain equations.

2.2. Theoretical analysis of sensing element

Fig. 2 shows the schematic diagram of the sensing element (rectangular taper beam). The equations are derived for analyzing the strain distribution of the rectangular beams (sensing elements) in size of thickness t_1 and width b_1. Then, the equations for analyzing the strain distribution of the rectangular taper beams (sensing elements) in size of thickness t_1, t_1' and width b_1, b_1' are used as those equations for the rectangular beams by substituting thickness t_1, t_1' and width b_1, b_1' for thickness t_1 and width b_1. The equations for thickness t_{1x} and width b_{1x} at arbitrary point x in length l_1 can be derived as

$$t_{1x} = t_1 + \frac{x}{l_1}(t_1' - t_1), \tag{1}$$

$$b_{1x} = b_1 + \frac{x}{l_1}(b_1' - b_1). \tag{2}$$

2.2.1 A case in which force Fy (or Fx) is applied to the sensor

Fig. 3 presents the free body diagram of the rectangular beams and PPBs under force Fy (or Fx). When the force Fx or Fy applies to the force/moment transmitting block respectively, the sensing elements for Fx sensor are the rectangular beam F and G, and

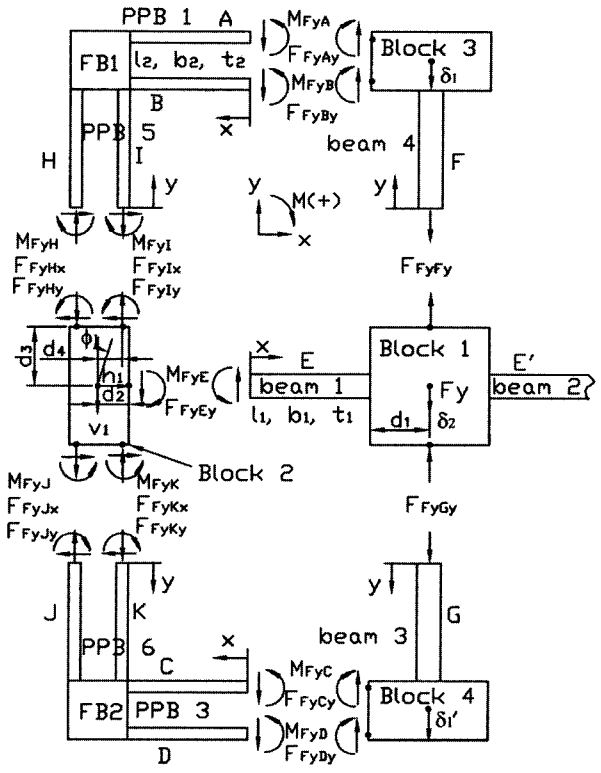

Fig. 3. Free body diagram of the rectangular taper beams and PPBs under force Fy (or Fx).

those for Fy sensor are the rectangular beam E and E′. As shown in Fig. 2, the rectangular beams and the PPBs are symmetrical on the basis of x-axis and y-axis. Thus, the equations for analyzing the strains on the left and the right surfaces of the rectangular beam E and E′ are derived. When the force-Fy applies to force/moment transmitting block, the displacement of the force/moment transmitting block, the moving blocks MB2 and MB4 are δ_2, δ_1, and δ_1' respectively. In addition, the rotational angle, the vertical displacement, and the horizontal displacement of the moving block MB1 are ϕ_1, v_1, and h_1 respectively.

By using the equilibrium-condition equations of moment and force at force/moment transmitting block and the moving block MB1, that is, $\sum Fx = 0$, $\sum Fy = 0$ and $\sum M = 0$, the equations lead to

$$2F_{FyFy} + 2F_{FyEy} = Fy, \tag{3}$$

$$F_{FyJx} + F_{FyKx} - F_{FyHx} - F_{FyIx} = 0, \tag{4}$$

$$F_{FyIy} + F_{FyKy} - F_{FyHy} - F_{FyJy} - F_{FyEy} = 0, \tag{5}$$

$$M_{FyE} - M_{FyI} - M_{FyH} - M_{FyK} - M_{FyJ} + d_2F_{FyEy} - 2d_4F_{FyIy} - 2d_4F_{FyHy} - 2d_3F_{FyIx} - 2d_3F_{FyKx} = 0. \tag{6}$$

The equations of the force applied to the beam A and B of PPB 1 along the y-axis F_{FyAy} and F_{FyBy}, the force applied to the rectangular beam F along the y-axis F_{FyFy}, the moment applied to the beam A and B of PPB 1 M_{FyA} and M_{FyB}, the force and moment applied to the rectangular beam E along the y-axis F_{FyEy} and M_{FyE}, the force applied to the PPB beam I along the y-axis and the x-axis F_{FyIy} and F_{FyIx}, the moment applied to the PPB beam I M_{FyI}, the force applied to the PPB beam K along the y-axis and the x-axis F_{FyKy} and F_{FyKx}, and the moment applied to the PPB beam K M_{FyK} can be derived, and substituting these force equations and moment equations into (3), (4), (5), and (6), the equations can be obtained as

$$k_{11}\delta_2 + k_{12}v_1 + k_{13}\phi_1 = Fy, \tag{7}$$

$$k_{14}\delta_2 + k_{15}v_1 + k_{16}\phi_1 = 0, \tag{8}$$

$$k_{17}\delta_2 + k_{18}v_1 + k_{19}\phi_1 = 0, \tag{9}$$

where $k_{11} \sim k_{19}$ are the constants, respectively. They are

$$k_{11} = \frac{2}{\frac{l_1}{A_1E} + \frac{l_2^3}{48EI_2}} + \frac{24EI_2}{l_1^3}, \quad k_{12} = -\frac{24EI_1}{l_1^3},$$

$$k_{13} = -\frac{24EI_1}{l_1^3}(d_2 + \frac{l_1}{2}), \quad k_{14} = -\frac{24EI_1}{l_1^3},$$

$$k_{15} = \frac{4A_2E}{l_2} + \frac{24EI_1}{l_1^3}, \quad k_{16} = \frac{12EI_1}{l_1^3}(d_2 + \frac{l_1}{2}),$$

$$k_{17} = \frac{24EI_1}{l_1^2} + \frac{12EI_1d_2}{l_1^3}, \quad k_{18} = \frac{6EI_1}{l_1^2} - \frac{12EI_1d_2}{l_1^3},$$

$$k_{19} = -\left[\begin{array}{l} \frac{12EI_1}{l_1^2}(\frac{d_2}{2} + \frac{l_1}{3}) + \frac{48EI_2}{l_2^2}(\frac{d_3}{2} + \frac{l_2}{3}) + \frac{12EI_1d_2}{l_1^3} \\ \times(d_2 + \frac{l_1}{2}) + \frac{4AEI_2d_4}{l_2} + \frac{48EI_2d_4}{l_2^3}(d_3 + \frac{l_2}{2}) \end{array}\right],$$

where l_1 is the length of the rectangular beam, l_2 is the length of the beam of PPBs, $A_1 = b_1t_1$ is the area of the rectangular beam, A_2 is the area of the PPB beam, $I_1 = \frac{b_1t_1^3}{12}$ is the moment of inertia of the area of the rectangular beam under force Fy, $I_2 = \frac{b_2t_2^3}{12}$ is the moment of inertia of the area of the PPB beam under force Fy, E is the modulus of longitudinal elasticity, δ_2 is vertical displacement of force/

moment transmitting block under force Fy, h_1 is the horizontal displacement of MB1 under force Fy, v_1 is the vertical displacement of MB 1 under force Fy, ϕ_1 is the rotational angle of MB1 under force Fy, d_2 is a half of the width of MB1, d_3 is a half of the height of MB1, and d_4 is the distance from the center point of MB1 to the centerline of the PPB beam I.

The equations for analyzing the strains on the left and right surfaces of the rectangular beam E and E′ are derived by using the bending moment, which can be written as

$$\varepsilon_{FyE\_upper} = \frac{12I_1 x}{l_1^3 z_{p1}}\left(\delta_2 - v_1 - (d_2 + \frac{l_1}{2})\phi_1\right) - \frac{12I_1}{l_1^2 z_{p1}}\left(\frac{\delta_2}{2} - \frac{v_1}{2} - (\frac{d_2}{2} + \frac{l_1}{3})\phi_1\right), \quad (10)$$

$$\varepsilon_{FyE\_lower} = -\frac{12I_1 x}{l_1^3 z_{p1}}\left(\delta_2 - v_1 - (d_2 + \frac{l_1}{2})\phi_1\right) + \frac{12I_1}{l_1^2 z_{p1}}\left(\frac{\delta_2}{2} - \frac{v_1}{2} - (\frac{d_2}{2} + \frac{l_1}{3})\phi_1\right), \quad (11)$$

where $z_{p1} = \frac{b_1 t_1^2}{6}$ is the polar moment of inertia of the rectangular beams.

2.2.2 A case in which force Fz is applied to the sensor

Fig. 4 shows the free body diagram of the rectangular beam under force Fz/4. By using the moment equilibrium-condition at the moving block MB1, that is, $\sum M = 0$, the equation leads to

$$d_2 F_{FzEy} + M_{FzE} - M_{Fz2} = 0. \quad (12)$$

The equations of the force and the moment applied to the rectangular beam E along the y-axis F_{FzEy} and M_{FzE}, and the twist moment of PPB5 and 6 M_{Fz2} can be derived, and substituting these force equations and moment equations into (12), the equations can be written as

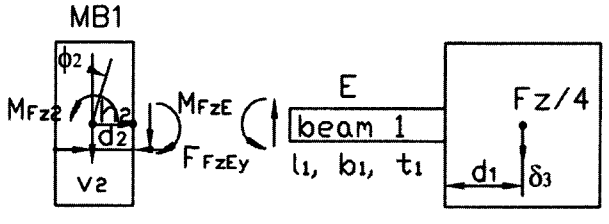

Fig. 4. Free body diagram of the rectangular beam under force Fz/4.

$$k_{21}\delta_3 + k_{22}\phi_2 = \frac{12EI_{21}d_2 v_2}{l_1^3} - \frac{6EI_{21}v_2}{l_1^2}, \quad (13)$$

$$k_{23}\delta_3 + k_{24}\phi_2 = \frac{Fz}{4} + \frac{12EI_{21}v_2}{l_1^3}, \quad (14)$$

where the vertical displacement of MB1 is $v_2 = \frac{Fzl_2^3}{16Et_2b_2^3}$, and $k_{21} \sim k_{24}$ are the constants respectively. They are

$$k_{21} = \frac{12EI_{21}d_2}{l_1^3} + \frac{6EI_{21}}{l_1^2},$$

$$k_{22} = -\frac{12EI_{21}d_2}{l_1^3}(d_2 + \frac{l_1}{2}) - \frac{12EI_{21}}{l_1^2}(\frac{d_2}{2} + \frac{l_1}{3}) - \frac{2G}{\frac{d_3}{I_{PB}} + \frac{l_2}{I_{P2}}},$$

$$k_{23} = \frac{12EI_{21}}{l_1^3},\ k_{24} = -\frac{12EI_{21}}{l_1^3}(d_2 + \frac{l_1}{2}),$$

where δ_3 is the vertical displacement of MB1 under force Fz/4, v_2 is the vertical displacement of MB1 under force Fz/4, ϕ_2 is the rotational angle of MB1 under force Fz/4, and $I_{21} = \frac{t_1 b_1^3}{12}$ is the moment of inertia of the area of the rectangular beam, G is the modulus of torsion elasticity, $I_{PB} = \frac{d_2 b_2^3}{6} + \frac{2b_2 d_2^3}{3}$ is the moment of inertia of the area of MB1, and $I_{P2} = \frac{2t_2 b_2^3}{12} + \frac{b_2\left[(2d_2)^3 - (2d_2 - 2t_2)^3\right]}{12}$ is the moment of inertia of the area of PPB 5 and 6 under force Fz/4.

The equations for analyzing the rated strains on the upper and lower surfaces of the rectangular beam E and E′ are derived by using the bending moment, which can be written as

$$\varepsilon_{FyE\_upper} = \frac{12I_{21}x}{l_1^3 z_{p21}}\left(\delta_3 - v_2 - (d_2 + \frac{l_1}{2})\phi_2\right) - \frac{12I_{21}}{l_1^2 z_{p21}}\left(\frac{\delta_3}{2} - \frac{v_2}{2} - (\frac{d_2}{2} + \frac{l_1}{3})\phi_2\right), \quad (15)$$

$$\varepsilon_{FyE\_lower} = -\frac{12I_{21}x}{l_1^3 z_{p21}}\left(\delta_3 - v_2 - (d_2 + \frac{l_1}{2})\phi_2\right) + \frac{12I_{21}}{l_1^2 z_{p21}}\left(\frac{\delta_3}{2} - \frac{v_2}{2} - (\frac{d_2}{2} + \frac{l_1}{3})\phi_2\right), \quad (16)$$

where $z_{p21} = \frac{t_1 b_1^2}{6}$ is the polar moment of inertia of the rectangular beam under force Fz/4.

2.2.3 A case in which moment My (or Mx) is applied to the sensor

Fig. 5 indicates the free body diagram of the rectangular beams under moment My/2 (or Mx/2). By using the moment equilibrium-condition at force/moment transmitting block and the moving block MB1, that is, $\sum M = 0$, the equations lead to

$$(l_1 + d_1)F_{MyEy} - M_{MyE} + \frac{M_{My1}}{2} = \frac{My}{2}, \tag{17}$$

$$d_2 F_{MyEy} + M_{MyE} - M_{My2} = 0, \tag{18}$$

$$\frac{4Et_2 b_2^3 v_3}{l_2^3} = \frac{12EI_1}{l_1^3}\left((d_1 + \frac{l_1}{2})\theta_3 - v_3 - (d_2 - \frac{l_1}{2})\phi_3\right). \tag{19}$$

The equations of the force applied to the rectangular beam E along the y-axis F_{MyEy} and the moment applied to the rectangular beam E M_{MyE}, the twist moment of PPB5 and 6 can be derived, and substituting these force equations and moment equations into (17), (18), and (19), the equations can be expressed as

$$k_{31}\theta_3 + k_{32}v_3 + k_{33}\phi_3 = \frac{My}{2}, \tag{20}$$

$$k_{34}\theta_3 + k_{35}v_3 + k_{36}\phi_3 = 0, \tag{21}$$

$$k_{37}\theta_3 + k_{38}v_3 + k_{39}\phi_3 = 0, \tag{22}$$

where $k_{31} \sim k_{39}$ are the constants, respectively. They are

$$k_{31} = \frac{12EI_{21}}{l_1^3}(d_1 + l_1)(d_1 + \frac{l_1}{2}) - \frac{12EI_{21}}{l_1^2}(\frac{d_1}{2} + \frac{l_1}{3}) + \frac{2GI_{P1}}{l_1},$$

$$k_{32} = \frac{12EI_{21}}{l_1^3}(d_1 + l_1) + \frac{6EI_{21}}{l_1^2},$$

$$k_{33} = -\frac{12EI_{21}}{l_1^3}(d_1 + l_1)(d_2 - \frac{l_1}{2}) + \frac{12EI_{21}}{l_1^2}(\frac{d_1}{2} - \frac{l_1}{3}),$$

$$k_{34} = \frac{12EI_{21}d_2}{l_1^3}(d_1 + \frac{l_1}{2}) + \frac{12EI_{21}}{l_1^2}(\frac{d_1}{2} + \frac{l_1}{3}),$$

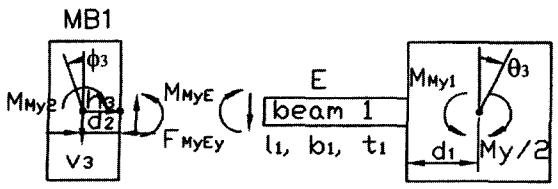

Fig. 5. Free body diagram of the rectangular beams under moment My/2 (or Mx/2).

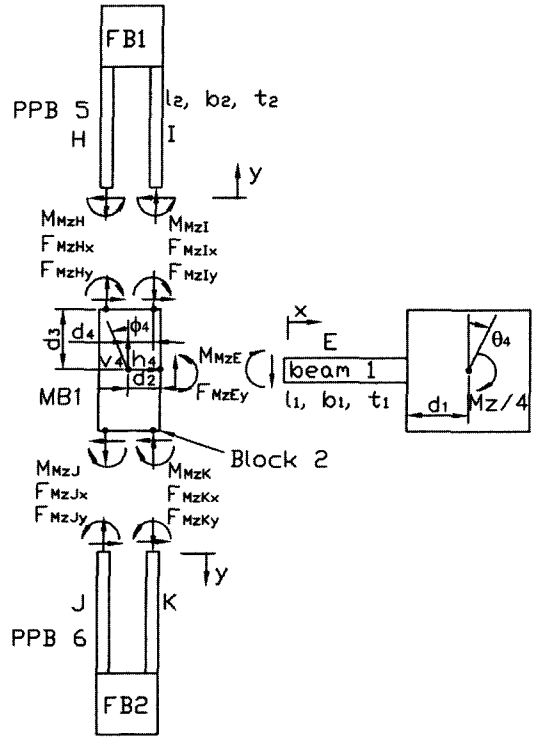

Fig. 6. Free body diagram of the rectangular beam and PPBs under moment Mz.

$$k_{35} = -\frac{12EI_{21}d_2}{l_1^3} - \frac{12EI_{21}}{l_1^2},$$

$$k_{36} = \frac{12EI_{21}d_2}{l_1^3}(d_2 - \frac{l_1}{2}) - \frac{12EI_{21}}{l_1^2}(\frac{d_2}{2} - \frac{l_1}{3}) - \frac{2G\phi_3}{\frac{d_3}{I_{PB}} + \frac{l_2}{I_{P2}}},$$

$$k_{37} = \frac{12EI_{21}}{l_1^3}(d_1 + \frac{l_1}{2}),$$

$$k_{38} = -\frac{12EI_{21}}{l_1^3} - \frac{4Et_2 b_2^3}{l_2^3}, \quad k_{39} = \frac{12EI_{21}}{l_1^3}(d_1 - \frac{l_1}{2}),$$

where d_1 is a half of the width of MB1, θ_3 is the rotational angle of MB1 under moment My/2, v_3 is the vertical displacement of MB1 under moment My/2, and ϕ_3 is the rotational angle of MB1 under moment My/2.

The equations for analyzing the strains on the upper and lower surfaces of the rectangular beam E and E′ are derived by using the bending moment, which can be written as

$$\varepsilon_{FyE\_upper} = \frac{12I_{21}x}{l_1^3 z_{p21}}\left((d_1 + \frac{l_1}{2})\theta_3 - v_3 - (d_2 - \frac{l_1}{2})\phi_3\right) - \frac{12I_{21}}{l_1^2 z_{p21}}\left((\frac{d_1}{2} + \frac{l_1}{3})\theta_3 - \frac{v_3}{2} - (\frac{d_2}{2} - \frac{l_1}{2})\phi_3\right), \tag{23}$$

$$\varepsilon_{FyE\_lower} = -\frac{12I_{21}x}{l_1^3 z_{p21}}\left((d_1+\frac{l_1}{2})\theta_3 - v_3 - (d_2-\frac{l_1}{2})\phi_3\right) + \frac{12I_{21}}{l_1^2 z_{p21}}\left((\frac{d_1}{2}+\frac{l_1}{3})\theta_3 - \frac{v_3}{2} - (\frac{d_2}{2}-\frac{l_1}{2})\phi_3\right). \quad (24)$$

2.2.4 A case in which moment Mz is applied to the sensor

Fig. 6 shows the free body diagram of the rectangular beam and PPBs under moment Mz/4. By using the equilibrium-condition equations of moment and force at force/moment transmitting block and the moving block MB1, that is, $\sum Fx = 0$, $\sum Fy = 0$, and $\sum M = 0$, the equations lead to

$$F_{MzEy}(l_1+d_1) - M_{MzE} = \frac{Mz}{4}, \quad (25)$$

$$2F_{MzHx} - 2F_{MzJx} = 0, \quad (26)$$

$$2F_{MzHy} - 2F_{MzIy} + F_{MzEy} = 0, \quad (27)$$

$$M_{MzE} - M_{MzI} - M_{MzJ} - M_{MzK} + d_2F_{MzEy} - d_3F_{MzHx} - d_3F_{MzIx} - d_3F_{MzJx} - d_3F_{MzKx} - d_4F_{MzHy} - d_4F_{MzIy} - d_4F_{MzJy} - d_4F_{MzKy} = 0. \quad (28)$$

The equations of the force applied to the rectangular beam E along the y-axis F_{MzEy} and the moment applied to the rectangular beam E M_{MzE}, the force applied to the rectangular beam I, H, J and K along the y-axis F_{MzIy}, F_{MzHy}, F_{MzJy}, F_{MzKy}, the force applied to the rectangular beam I, H, J and K along the x-axis F_{MzIx}, F_{MzHx}, F_{MzJx}, F_{MzKx}, and the moment applied to the rectangular beam I, H, J and K, M_{MzI}, M_{MzH}, M_{MzJ}, M_{MzK} respectively can be derived, and substituting these force equations and moment equations into (25), (26), (27), and (28), the equations can be written as

$$k_{41}\theta_4 + k_{42}v_4 + k_{43}\phi_4 = \frac{Mz}{4}, \quad (29)$$

$$k_{44}\theta_4 + k_{45}v_4 + k_{46}\phi_4 = 0, \quad (30)$$

$$k_{47}\theta_4 + k_{48}v_4 + k_{49}\phi_4 = 0, \quad (31)$$

where $k_{41} \sim k_{49}$ are the constants, respectively. They are

$$k_{41} = \frac{12EI_1}{l_1^3}(d_1+l_1)(d_1+\frac{l_1}{2}) - \frac{12EI_1}{l_1^2}(\frac{d_1}{2}+\frac{l_1}{3}),$$

$$k_{42} = -\frac{12EI_1}{l_1^3}(d_1+l_1) + \frac{6EI_1}{l_1^2},$$

$$k_{43} = \frac{12EI_1}{l_1^3}(d_1+l_1)(d_2-\frac{l_1}{2}) - \frac{12EI_1}{l_1^2}(\frac{d_2}{2}-\frac{l_1}{3}),$$

$$k_{44} = \frac{12EI_1}{l_1^3}(d_1+\frac{l_1}{2}), \quad k_{45} = -\frac{4A_2E}{l_2} - \frac{12EI_1}{l_1^3},$$

$$k_{46} = -\frac{12EI_1}{l_1^3}(d_2-\frac{l_1}{2}),$$

$$k_{47} = \frac{12EI_1}{l_1^3}(\frac{d_1}{2}+\frac{l_1}{3}) + \frac{12EI_1d_2}{l_1^3}(d_1+\frac{l_1}{2}),$$

$$k_{48} = \frac{6EI_1}{l_1^2} - \frac{12EI_1d_2}{l_1^3},$$

$$k_{49} = -\frac{12EI_1}{l_1^3}(\frac{d_2}{2}-\frac{l_1}{3}) - \frac{48EI_2}{l_2^3}(\frac{d_2}{2}+\frac{l_2}{3}) - \frac{12EI_1d_2}{l_1^3}(d_2-\frac{l_1}{2}) - \frac{48EI_2d_3}{l_2^3}(d_3+\frac{l_2}{2}) - \frac{4A_2Ed_4^2}{l_2},$$

where θ_4 is the rotational angle of MB1 under moment Mz/4, v_4 is the vertical displacement of MB1 under moment Mz/4, ϕ_4 is the rotational angle of MB1 under moment Mz/4, and h_4 is the horizontal displacement of MB1 under moment Mz/4.

The equations for analyzing the strains on the upper and lower surfaces of the rectangular beam E and E′ are derived by using the bending moment, which can be written as

$$\varepsilon_{MzE\_upper} = \frac{12I_1x}{l_1^3 z_{p1}}\left((d_1+\frac{l_1}{2})\theta_4 - v_4 - (d_2-\frac{l_1}{2})\phi_4\right) - \frac{12I_1}{l_1^2 z_{p1}}\left((\frac{d_1}{2}+\frac{l_1}{3})\theta_4 - \frac{v_4}{2} - (\frac{d_2}{2}-\frac{l_1}{2})\phi_4\right), \quad (32)$$

$$\varepsilon_{MzE\_lower} = -\frac{12I_1x}{l_1^3 z_{p1}}\left((d_1+\frac{l_1}{2})\theta_4 - v_4 - (d_2-\frac{l_1}{2})\phi_4\right) + \frac{12I_1}{l_1^2 z_{p1}}\left((\frac{d_1}{2}+\frac{l_1}{3})\theta_4 - \frac{v_4}{2} - (\frac{d_2}{2}-\frac{l_1}{2})\phi_4\right). \quad (33)$$

2.3. Design of sensor

The design variables of the modeled six-axis force/moment sensor are the size of body, the rated load and output of each sensor, the sizes of rectangular taper beams with width b_1 and b_1', the thickness t_1 and t_1', and the length l_1, the sizes of PPBs with width b_2, the thickness t_2 and the length l_2, and the gap a between two parallel plates of PPBs.

Thus, in this paper, in the first place, the rated output of each sensor is determined by 0.5 mV/V (calculated by (34) and (35)), the rated loads of Fx sensor, Fy sensor and Fz sensor are all 200N, those of Mx sensor and My sensor are 2.5Nm, and

that of Mz sensor is 5.0Nm. The diameter of a fixture ring is 100mm, the size of rectangular-shaped consisted of PPBs is 74mm, the height of the sensor is 31 mm, the diameter of a force/moment transmitting block is 30 mm, the attachment position of strain-gage is 3mm or 5mm, and the rated strain is 250μm/m.

Moreover, the length l_1 of a rectangular taper beam and the length l_2 of a PPB are determined by 14mm in consideration of the size of the sensing elements and strain-gages to attach, and the sizes of width b_1 and b_1', thickness t_1 and t_1', width b_2, thickness t_2, gap a are determined from theoretical analysis. Each sensor of the six-axis ankle force/moment sensor is fabricated by attaching strain-gages on the sensing element of each sensor, and composed by Wheastone bridge using the attached strain-gages.

The rated output in the rated load is determined from the strain values of the attached strain-gages. Total strain of Wheastone bridge can be calculated using the following equation

$$\varepsilon = \varepsilon_{T1} - \varepsilon_{C1} + \varepsilon_{T2} - \varepsilon_{C2}, \tag{34}$$

where ε is total strain from Wheastone bridge, ε_{T1} is strain of a tension strain-gage T_1, ε_{C1} is strain of a compression strain-gage C_1, ε_{T2} is strain of a tension strain-gage T_2, and ε_{C2} is strain of a compression strain-gage C_2.

Also, the rated output can be calculated as the equation below

$$\frac{E_o}{E_i} = K\varepsilon, \tag{35}$$

where E_i is the input voltage of Wheastone bridge, E_o is the output voltage of Wheastone bridge, K is the factor of strain-gage (about 2.0), ε is total strain derived from (34). The sizes of the sensing elements were calculated by substituting the determined variables into (10), (11), (15), (16), (23), (24), (32), and (33). The sizes of the sensing elements of the rectangular taper beam are the width b_1 of 4.4mm and b_1' of 4.9mm, t_1 of 4.1mm and t_1' of 3.4mm, thickness t_2 of 1.3mm, b_2 of 15mm, and the gap a of 5.4mm. The sizes of the sensing elements of the rectangular beam are the width $b_1 = b_1'$ of 3.8mm, thickness $t_1 = t_1''$ of 4.6mm, b_2 of 15mm, thickness t_2 of 1.3mm and the gap a of 5.4mm.

3. ATTACHMENT POSITION OF STRAIN-GAGES AND RESULTS OF THEORETICAL ANALYSIS

Fig. 7 indicates the attachment location of strain-gages for each sensor. The attachment location of strain-gages for Fx sensor is S1~S4, that for Fy sensor is S5~S8, that for Fz sensor is S9~S12, that for Mx sensor is S13~S16, that for My sensor is S17~S20 and that for Mz sensor is S21~S24. The attachment location of strain-gages is 3mm and 5mm along the length-direction from the force/moment transmitting block, and the centerline at width-direction. It is determined to get the maximum rated strain and interference error of 0% in consideration of the size of the used strain-gage.

The theoretical analysis program was made using the derived equations ((10), (11), (15), (16), (23), (25), (32) and (33)) by Excel Software (Microsoft), and the six-axis force/moment sensor was designed by using the program. Table 1 shows the strains of the sensing elements with rectangular taper beams from theoretical analysis and the calculated strains due to (34) at the attachment location of each strain-gage. The rated strain of Fx sensor or Fy sensor is all 1000μm/m, that of Fz sensor is 1002μm/m, that of Mx sensor or My sensor is all 1004μm/m and that of Mz sensor is 1010μm/m. Table 2 reveals the strains of the sensing elements with the rectangular beams from theoretical analysis and the calculated strains due to (34) at the attachment location of each strain-gage. The rated strain of Fx sensor or Fy sensor is all 1004μm/m, that of Fz sensor is 1002μm/m,

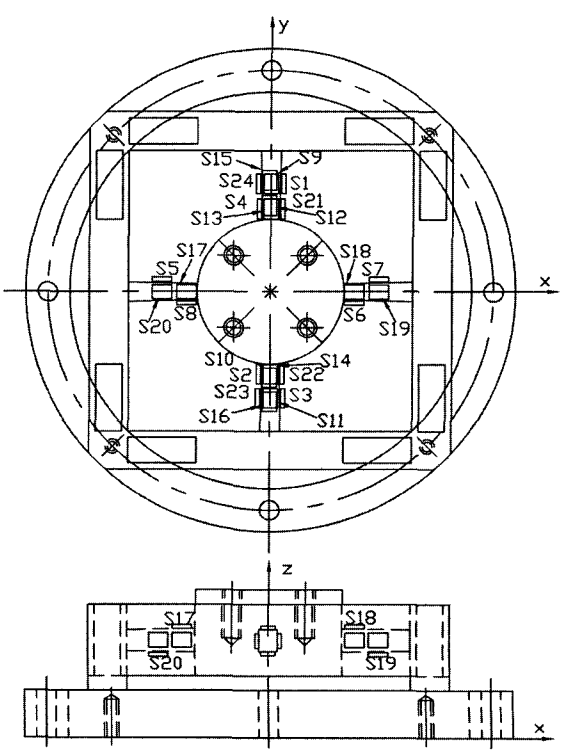

Fig. 7. Attachment location of strain-gages for each sensor.

Table 1. Strains in the attachment location of strain-gages for each sensor.

Sensor	Strain (μm/m)				
	T_1	C_1	T_2	C_2	ε
Fx	194	-306	194	-306	1000
Fy	194	-306	194	-306	1000
Fz	185	-316	185	-316	1002
Mx	320	-320	186	-186	1012
My	320	-320	186	-186	1012
Mz	317	-317	188	-188	1010

Table 2. Strains in the attachment location of strain-gages for each sensor.

Sensor	Strain (μm/m)				
	T_1	C_1	T_2	C_2	ε
Fx	182	-320	182	-320	1004
Fy	182	-320	182	-320	1004
Fz	198	-303	198	-303	1002
Mx	341	-341	215	-215	1112
My	341	-341	215	-215	1112
Mz	345	-345	205	-205	1105

that of Mx sensor or My sensor is all 1112 μm/m and that of Mz sensor is 1105 μm/m. The rated strain error of the modeled six-axis force/moment sensor with the rectangular taper beam was less than 1.2%, and that of the rectangular beam was less than 11.2%. It shows that the modeled six-axis force/moment sensor with the rectangular taper beam has more results, because the rectangular taper beam could be changed from t_1 to t_1' in thickness, and from b_1 to b_1' in width as shown in Fig. 2.

Thus, the six-axis force/moment sensor with rectangular taper beams can be designed more precisely than rectangular beams in the rated output of each sensor. And, the theoretical analysis program made of the derived equations can be used to design the modeled six-axis force/moment sensor.

4. FABRICATION OF SENSOR, RESULTS AND CONSIDERATION OF CHARACTERISTIC TEST

The six-axis force/moment sensor was fabricated by attaching strain-gages at their locations and constructing the Wheastone bridge of each sensor. The used strain-gage (N2A-13-S1452-350) is manufactured in the Micro-Measurement Company, its gage factor is 2.06 and size is 3×7.2mm. The used bond (M-bond 200) is also manufactured in the Micro-Measurement Company. The photograph of the fabricated six-axis force/moment sensor is shown in Fig. 8. The manufactured six-axis force/moment sensor must be carried out by the characteristic test using the six-component force/moment sensor testing machine [13] to evaluate its rated output under each rated load, which are forces Fx=Fy=Fz=200N and moments Mx=My=2.5Nm, Mz=5.0Nm. Each sensor was tested three times by using the testing machine, and the output values from each sensor were averaged.

Table 3 shows the rated outputs from the results of theoretical analysis and characteristic test. The rated output from theoretical analysis is the values calculated from (35). That for Fx sensor, Fy sensor, Fz sensor, Mx sensor, My sensor and Mz sensor is 0.515 mV/V, 0.515 mV/V, 0.516 mV/V, 0.521 mV/V, 0.521mV/V and 0.520mV/V respectively. The rated outputs from characteristic test of Fx sensor, Fy sensor, Fz sensor, Mx sensor, My sensor and Mz sensor are 0.503mV/V, 0.510mV/V, 0.499 mV/V, 0.537mV/V, 0.540mV/V and 0.538mV/V respectively. When the result from the characteristic test was compared with that from theory analysis, the error of the rated output of Fx sensor was 2.33%, that of Fy sensor was 0.97%, that of Fz sensor was 3.29%, that of Mx sensor was 3.07%, that of My sensor was

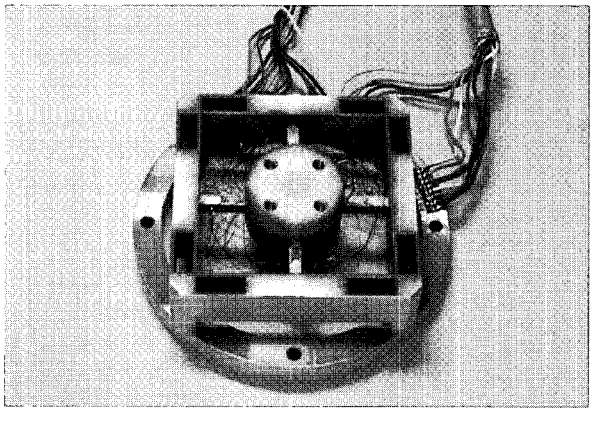

Fig. 8. Photograph of developed six-axis ankle force/moment sensor with rectangular taper beams.

Table 3. Rated output from theory analysis and characteristic test of each sensor.

Sensor	Rated output (mV/V)		
	Theory	Exp.	Error(%)
Fx	0.515	0.503	2.33
Fy	0.515	0.510	0.97
Fz	0.516	0.499	3.29
Mx	0.521	0.537	3.07
My	0.521	0.540	3.65
Mz	0.520	0.538	3.46

Table 4. Interference error of each sensor.

Sensor / F(N) /M(Nm)	Interference error (%)					
	Fx	Fy	Fz	Mx	My	Mz
Fx=200	-	0.75	0.24	0.28	-2.81	2.31
Fy=200	0.91	-	0.19	2.65	0.46	-0.26
Fz=200	2.35	0.27	-	-1.15	1.81	0.71
Mx=2.5	0.23	-2.21	1.02	-	-0.19	-0.62
My=2.5	1.74	-0.83	0.46	0.36	-	1.38
Mz=5.0	2.87	1.43	0.87	0.67	0.43	-

3.65% and that of Mz sensor was 3.46%. These errors are because of the attaching error of strain-gages (attachment location of strain-gages is 3mm and 5mm in length-direction from the force/moment transmitting block, and the centerline in width-direction), the machining error of the sensing element size (t_1 to t_1' in thickness, and from b_1 to b_1' in width), and so on. To get the rated output of above 0.500 mV/V from the theoretical analysis in each sensor, it is designed with four rectangular taper beams in the same size.

Table 4 shows the interference error of each sensor. The maximum interference error of the developed six-axis ankle force/moment sensor was less than 2.87%. Thus, it is thought that the sensor can be used for an intelligent robot's wrist and ankle.

5. CONCLUSIONS

In this paper, the six-axis ankle force/moment sensor with the rectangular taper beams was newly developed for an intelligent robot's foot. It was confirmed that the derived equations ((10), (11), (15), (16), (23), (24), (32), and (33)) could be used for designing the modeled six-axis ankle force/moment sensor with the rectangular taper beams, and the theoretical analysis program made of the derived equations can be used to design the sensor. The six-axis force/moment sensor with rectangular taper beams can be designed more precisely than rectangular beams in the rated output of each sensor. The interference error of the developed sensor from the characteristic test is less than 2.87%. It is estimated that the interference error of the sensor is similar to that of the existing sensor produced from the developed country. The size of the body of the six-axis force/moment sensor has the diameter of 100mm and the height of 32mm. Thus, it is thought that the developed six-axis force/moment sensor can be used for the intelligent wrist and ankle of an intelligent robot.

REFERENCES

[1] A. Morales, P. J. Sanz, A. P. Pobil, and A. H. Fagg, "Vision-based three-finger grasp synthesis constrained by hand geometry," *Robotics and Autonomous Systems*, vol. 54, no. 6, pp. 496-512, 2006.

[2] D. Osswald, J. Martin, C. Burghart, R. Mikut, H. Wörn, and G. Bretthauer, "Integrating a flexible anthropomorphic, robot hand into the control, system of a humanoid robot," *Robotics and Autonomous Systems*, vol. 48, no. 4, pp. 213-221, 2004.

[3] J. J. Steil, F. Röthling, R. Haschke, and H. Ritter, "Situated robot learning for multi-modal instruction and imitation of grasping," *Robotics and Autonomous Systems*, vol. 47, no. 2-3, pp. 129-141, 2004.

[4] A. Chella, H. Džindo, I. Infantino, and I. Macaluso, "A posture sequence learning system for an anthropomorphic robotic hand," *Robotics and Autonomous Systems*, vol. 47, no. 2-3, pp. 143-152, 2004.

[5] H. Hirukawa, F. Kanehiro, K. Kaneko, S. Kajita, K. Fujiwara, Y. Kawai, F. Tomita, S. Hirai, K. Tanie, and T. Isozumi, "Humanoid robotics platforms developed in HRP," *Robotics and Autonomous Systems*, vol. 48, no. 4, pp. 165-175, 2004.

[6] S. Kagami, M. Mochimaru, Y. Ehara, N. Miyata, K. Nishiwaki, T. Kanade, and H. Inoue, "Measurement and comparison of humanoid H7 walking with human being," *Robotics and Autonomous Systems*, vol. 48, no. 4, pp. 177-187, 2004.

[7] Y. Ogura, S. Ando, H. O. Lim, and A. Takanishi, "Sensory-based walking motion instruction for biped humanoid robot," *Robotics and Autonomous Systems*, vol. 48, no. 4, pp. 223-230, 2004.

[8] J. F. Seara and G. Schmidt, "Intelligent gaze control for vision-guided humanoid walking: Methodological aspects," *Robotics and Autonomous Systems*, vol. 48, no. 4, pp. 231-248, 2004.

[9] G. S. Kim and H. D. Lee, "Development of a six-axis force/moment sensor and its control system for an intelligent robot's gripper," *Measurement Science and Technology*, vol. 14, pp. 1265-1274, 2003.

[10] G. S. Kim, "Development of a small six-axis force/moment sensor for robot's fingers," *Measurement Science and Technology*, vol. 15, pp. 2233-2238, 2004.

[11] G. S. Kim and J. J. Park, "Development of the six-axis force/moment sensor for an intelligent robot's gripper," *Sensors and Actuators*, vol. 118, pp. 127-134, 2005.

[12] ATI Industrial Automation, "Multi-axis force/torque sensor," ATI Industrial Automation, pp. 4-

45, 2005.
[13] G.-S. Kim, "The development of a six-component force/moment sensor testing machine and evaluation of its uncertainty," *Measurement Science and Technology*, vol. 11, pp. 1377-1382, 2000.

Gab-Soon Kim received the M.S. and Ph.D. degrees in Precision Mechanical Engineering from Hanyang University in 1990 and 1999, respectively. He was previously employed as a Senior Researcher in the Division of Mechanical Metrology, KRISS (Korea Research Institute of Standards Science), Taejon, Korea. Since 2000, he has been an Associate Professor at Gyeongsang National University. His research interests include the design of multi-axis force/moment sensor, intelligent system and control, service robots and humanoid robots.